Int J Adv Manuf Technol (2015) 80:301–314
DOI 10.1007/s00170-015-7007-4

ORIGINAL ARTICLE

Mechanical behaviour of friction stir spot welds of polycarbonate sheets

F. Lambiase[1] · **A. Paoletti**[1] · **A. Di Ilio**[1]

Received: 11 September 2014 / Accepted: 9 March 2015 / Published online: 24 March 2015

Abstract The present investigation is aimed at analyzing the influence of the processing speeds and processing times on mechanical behaviour of friction stir spot welding (FSSW) joints produced on polycarbonate sheets. The analysis involved the variation of rotational speed, tool plunge rate, pre-heating time, dwell time and waiting time. Mechanical characterization of joints was carried out by means of single lap shear test. Experimental tests were conducted according to two full factorial designs. First, an exploratory 2^5 full factorial plan was carried out to determine the most influencing factors determining the mechanical behaviour of FSSW joints. Then, a 3^3 optimization plan was performed by varying the most relevant process parameters among three levels. Therefore, analytical models were developed to predict the mechanical behaviour of welds (maximum shear strength, stiffness and absorbed energy) produced under different processing conditions. In addition, an artificial neural network (ANN) model was developed to improve the matching between experimental measurements and model predictions. On the basis of the achieved results, a framework for improving the mechanical performances of thermoplastic joints was established. According to the achieved results, tool plunge rate, dwell time and waiting time are the most influencing parameters for the joint strength and weld extension. On the other hand, pre-heating time and tool rotational speed have lower influence on the mechanical behaviour of FSSW joints.

✉ F. Lambiase
francesco.lambiase@univaq.it

[1] Dept. of Industrial and Information Engineering and Economics, University of L'Aquila, Via Campo di Pile, 67100, AQ L'Aquila, Italy

Keywords Friction stir spot welding · Joining · Polymers · Thermoplastics · Welding · Mechanical behaviour

1 Introduction

The employment of polymeric materials has been diffused among several industrial fields including electronics, automotive, aerospace and packaging. Joining polymer materials represents a critical step in the manufacture of complex assemblies. Several joining methods for similar and dissimilar polymer structures are used in the automotive industry [1, 2]. Clinching has been recently employed for joining polymers and metal sheets [3–5]; Liu et al. [6] employed friction lap welding for the same purpose. Among the processes which allow to join polymers as well as polymer-metals [7–12], friction stir spot welding (FSSW) produces weld with strength comparable or higher to other welding techniques, whilst joining times are equal or shorter [13]. FSSW joints are characterized by reduced distortion, no filler metal or shielding gas, the mechanical strength of joints is close to that of the base material, fatigue life is 2-10 times arc welding and no unsightly soot is produced. Moreover, the process is adaptable to all positions and it can be used to join numerous non-ferrous alloys (even those considered not weldable) and, at last, can weld a wide range of material thicknesses ranging from 1 to 50 mm [14].

Similarly to resistance spot welding (RSW), FSSW involves only the plunge and tool retraction; thus, it can be used to replace RSW, riveting, clinching or any other single point joining processes in many applications. FSSW was applied on metals, e.g. aluminium, magnesium and steel alloys sheets [15–18] but also on thermoplastic polymers [19, 20] and particularly on high-density polyethylene (HDPE), polypropylene (PP), polymethylmethacrylate (PMMA) and acrilonitrile

butadiene styrene (ABS) sheets [21–23]. Nevertheless, the thermo-mechanical conditions produced during FSW of polymers, material flow as well as welds defects are completely different from those occurring in metals owing to rheological and physical differences [24].

Prior studies mainly focussed on geometrical parameters optimization for increasing the mechanical properties of the welds. Dashatan et al. [25] investigated the effects of tool penetration depth and dwell time on mechanical properties of PMMA/ABS welds produced by FSSW. The most effective parameter was found to be tool plunge rate. Weld strength is enhanced by increasing the dwell time; on the contrary, it decreases by increasing the tool plunge rate. Armagan and Senol [26] determined the optimal tool penetration depth that maximizes joint tensile failure in friction stir spot welding of polypropylene. Oliviera et al. [27] developed a new tool, in which the pin and shoulder could rotate independent of each other: according to the authors' results, such configuration would lead to a decrease in weld imperfections and higher strengths. Although a number of investigations were carried out to study the influence of the process parameters in FSSW of thermoplastic polymers, they mainly focused on evaluating the influence of the tool tip geometry and only some of the processing speeds on the mechanical behaviour of FSSW joints. On the other hand, in the present study, the scope is to focus exclusively on the effect of the processing speeds and processing times whilst keeping constant the geometry and dimensions of the tool tip as well as the penetration depth. Analytical and experimental approaches were followed to assess the effect of rotational speed, tool plunge rate, pre-heating time, dwell time and waiting time on the mechanical behaviour and geometry of friction spot stir welds. Tensile tests were carried out to evaluate the main mechanical properties of the parent material whilst single lap shear tests were performed to evaluate the mechanical behaviour of FSSW joints. Cross sections of relevant joints were performed to investigate the influence of relevant process parameters on material flow produced by the FSSW process of thermoplastic materials. Finally, empirical and neural network models were developed to predict and control the shear strength of welded connections. Such models represent a useful tool for process planning in friction spot stir welding of thermoplastic materials.

2 Experiments

2.1 Characterization of parent material

Polycarbonate sheets (PC) of 3 mm in thickness were joined by friction spot stir welding. To compare the mechanical properties of the welded region with those of the parent material, uniaxial tensile tests, according to ASTM D638 standards, were performed. During such tests, digital image correlation (DIC) was used to measure the deformation.

2.2 Experimental set up

Friction spot stir welds were performed on a servo-drilling press, equipped with an asynchronous motor, driven by an inverter. The geometry of the tool was not varied among the experiments as well as the penetration depth, s=4.4 mm (reported in Fig. 1), since the aim of the work was to focus on the effect of the main tool speeds and processing times involved in the FSSW process. Thus, a flat-end tool tip with a shoulder diameter of 11 mm, a pin diameter of 5 mm and a pin length of 4.3 mm made of low carbon steel was utilized. A fastening plate with an 18-mm diameter bore at the centre (to permit the passing of the welding tool) was used to clamp the sheets during the welding process.

Figure 2 depicts the clamping system and the experimental apparatus involved. The axial tool plunge rate and the revolution spindle speed are regulated by means of the servo-system and the inverter, respectively.

The process starts by rotating the tool at a prescribed speed (n); the punch moves towards the upper sheet and exerts a holding pressure for a given pre-heating time T_P. The process proceeds by plunging the tool against the sheets (joining phase) with a constant plunging speed v_F; during this phase, part of the material is ejected from the welding area, as shown in Fig. 1. As soon as the tool shoulder enters in contact with the upper sheet, the punch axial motion is stopped, whilst the tool rotational speed continues (consolidation) for a prescribed dwell time T_D. Frictional heat is generated during plunging

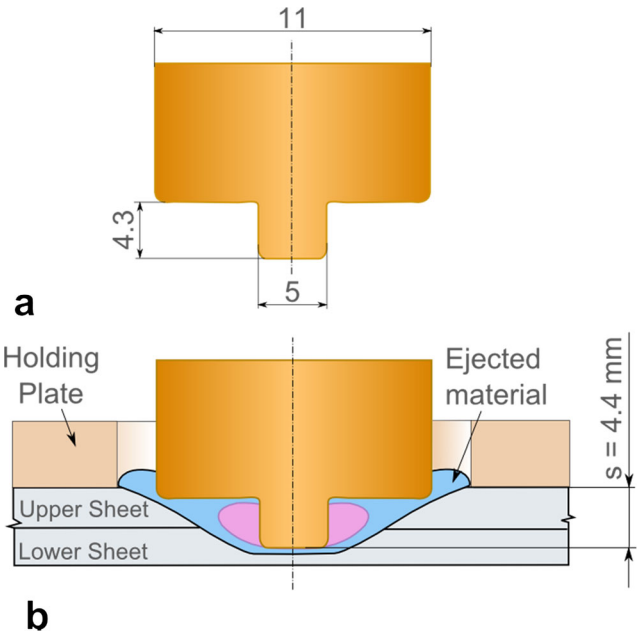

Fig. 1 **a** Schematic representation of FSSW tool and **b** clamping equipment near the welding region

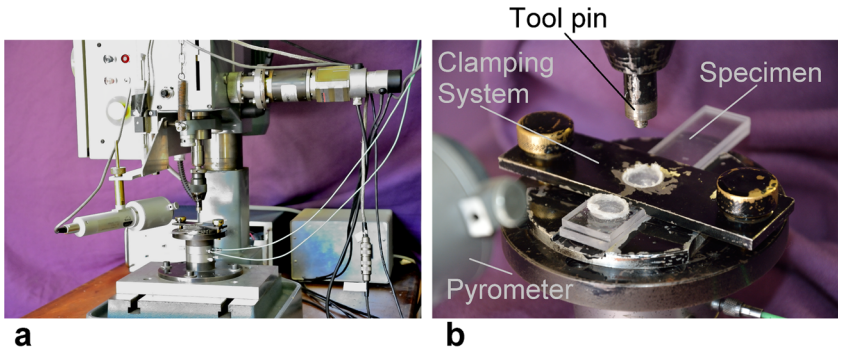

Fig. 2 Experimental apparatus **a** specimen clamping system and **b** servo-drilling machine

and stirring phases. Consequently, the material underlying and surrounding the tool is heated and softened as to be stirred by the tool. Then, the tool rotational speed is stopped and the punch is maintained at the joining depth. The tool shoulder compresses the underlying material; thus, after a waiting time T_W, the punch is retracted. The main phases are schematically depicted in Fig. 3.

2.3 Experimental procedure and plans

An exploratory 2^5 plan involving two-level full factorial design was carried out by varying tool plunge rate, tool rotation speed, pre-heating time, dwell time and waiting time. An additional 3^3 full factorial plan was carried out to investigate more in-depth the effects of the most significant factors in order to maximize the shear strength of the welds. In this case, the remaining factors were kept constant at the level that maximized the shear strength of the joint. The welding parameters and relative values employed in the 2^5 plan are summarized in Table 1. The levels of tool plunge rate and tool rotation speed were chosen in agreement with the drilling machine and control system limitations. The high levels of pre-heating time, dwell time and waiting time were set to the same value (20 s) in order to better evaluate the relative weight of each factor. Such a value was chosen on the basis of preliminary experimental tests and considering typical production needs (which aim to reduce the production time). The specimens were coded with the notation "$a_1a_2a_3a_4a_5$" whereas a_n ($n \leq 5$) equals −1 for lower level, 0 for the central point and +1 for higher level.

2.4 Characterization tests of FSSW welds

Single lap shear tests were carried out to determine the mechanical behaviour of welded joints on PC sheets. The samples for such tests were obtained by joining (with an overlapping length of 30 mm) rectangular sheets 90×20 mm cut from a unique sheet 2000×1000 mm using an alternative saw blade. The welds were performed at the centre of the overlapping area. Mechanical tests were performed at room temperature using a universal MTS 322.31 testing machine with 25 kN full-scale load at a constant cross head speed of 0.2 mm/min. Three replicates for each processing conditions were carried out. The cross sections of relevant specimens were analyzed by means of optical microscopy to investigate the influence of the process parameters on the mechanical performances of welds. Thus, dimensional characterization of the weld was

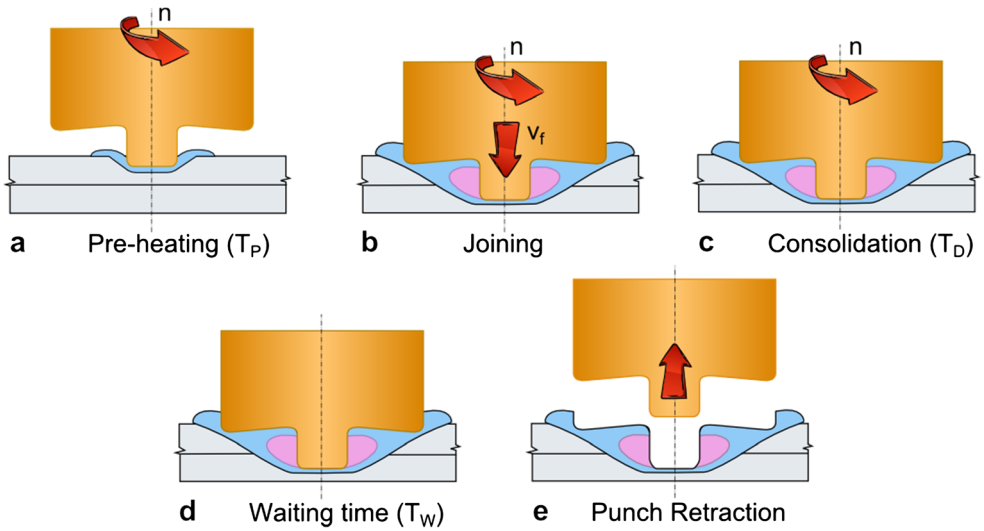

Fig. 3 Typical phases of friction stir spot welding process: **a** pre-heating, **b** joining, **c** consolidation, **d** waiting, and **e** tool retraction

Table 1 Experimental factors and levels used in the 2^5 exploratory plan

Symbol (n)	Welding parameter	Low level (−1)	High level (+1)
v_f (1)	Tool plunge rate (mm/min)	8	46
n (2)	Tool rotation speed (rpm)	1500	5400
T_P (3)	Pre-heating time (s)	0	20
T_D (4)	Dwell time (s)	0	20
T_W (5)	Waiting time (s)	0	20

performed for evaluating the extension of the welded area A_s (Fig. 4), in order to calculate the average shear stress of the joint $\sigma = F_r/A_s$.

3 Results and discussion

3.1 Mechanical behaviour of parent material

Figure 5 depicts the stress–strain curve of the analyzed material. The PC sheet was characterized by a yield stress of 60± 0.5 MPa, Young's modulus of 2.3 GPa and maximum elongation of 1.1.

3.2 Formation of a FSSW joint

During the joining phase, the rotating tool penetrates the heated and softened material which flows radially and upward. Under the effect of inertia forces, polymer particles are spun by the tool and ejected from the weld zone causing material loss in the welded bead. A flow zone of the base material is located near to the movement of the tool. Here, the polymer completely melted under the effect of the locally high temperature, flows and crystallizes along the shear rate direction. The weld zone is characterized by the width of the weld nugget x and the thickness of the upper sheet workpiece under the shoulder indentation y, as shown schematically in Fig. 6a.

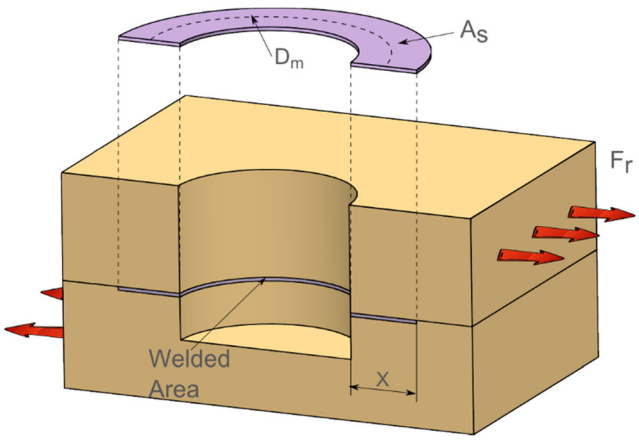

Fig. 4 Simplified model for calculation of mean shear stress of joints

The sizes of x and y determine the strength of the friction spot-welded joint.

To discern between the materials of the two sheets, a white-pigmented PC sheet was used as the lower sheet (tracer material) whilst a transparent PC sheet was used for the upper specimen. Figure 6b shows the cross section of a FSSW joint produced under optimal process parameters. As can be noted, two zones can be distinguished within the weld region, namely the upper-sheet reach zone (USRZ) and the Lower-sheet reach zone (LSRZ). The USRZ, which is almost transparent, is formed around the tool-pin and the layer underlying the tool shoulder; on the other hand, the LSRZ is formed surrounding the USRZ.

Unlike other plastic materials, polycarbonate tends to shrink significantly. This phenomenon increases the probability to produce internal cavities (during cooling). In the thickest areas of the joint, internal voids can arise due to the shrinkage prevented from the solidified skin. The inner material is torn, thus generating porosity. At low speeds, the tool tends to drag more easily the air during the joining phase. Nevertheless, porosities were observed in all sectioned specimens. In all the experimental tests, carried out by adopting low levels of pre-heating, dwell and waiting times, the presence of built up edge (BUE), as shown in Fig. 7, on both the pin surface and the frontal surface of the shoulder was found.

Built-up edge, which is formed by particles of the workpiece material, adhering to the tool surface, only occurs if:

- The chip formation is stable and largely stationary.
- There is a stagnant zone in the material flow in front of the tool surface.
- The temperatures in the chip formation zone are sufficiently low.

Built-up edge influences the pin geometry. During the process, the plastic material remains attached to the tool, resulting in a reduction of the internal diameter of the welded joint. Therefore, the formation of built-up edges is generally undesirable. However, it did not occur at higher pre-heating, dwell and waiting times and resulting higher temperatures in the chip formation zone.

3.3 Mechanical behaviour of FSSW joints

In order to highlight the relevance of the involved processing conditions, the force-displacement curves recorded during single lap shear test of FSSW joints realized by varying only the processing speeds and processing times are reported in Fig. 8a. As can be inferred, the choice of incorrect levels for the analyzed factors may dramatically compromise the mechanical behaviour of the welds.

The typical force-displacement curve and main mechanical behaviour of FWWS joints under shear load are schematically

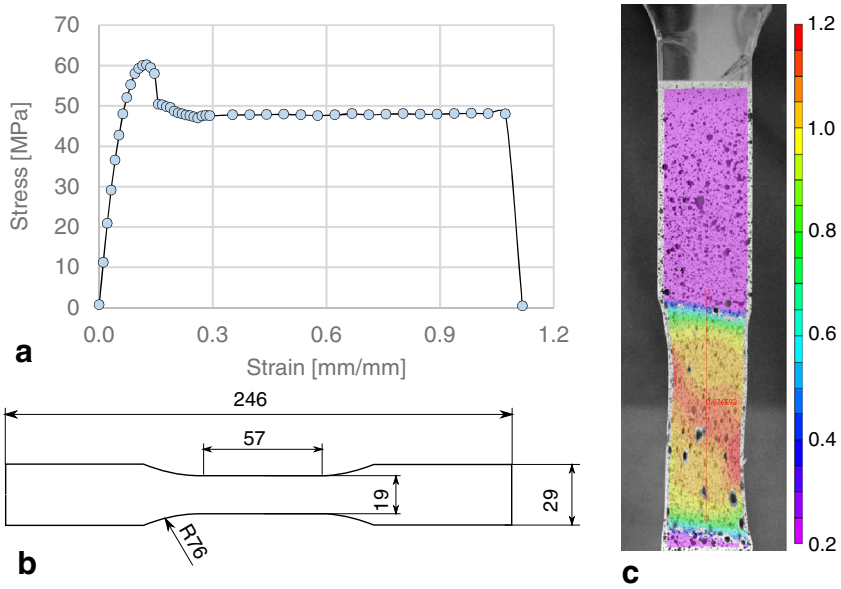

Fig. 5 Stress–strain curve of PC sheet recorded during uniaxial tensile tests

depicted in Fig. 8b. At the beginning of the test, the force increases almost linearly (the initial slope represents the joint stiffness, K) up to reaching a maximum value F_r (called shear strength) at a displacement d_r. As the test proceeds, the force reduces since the developing separation of the sheets. An initial fracture rising at the welded zone is followed by a sudden drop of the force up to the complete loss of the carrying load capability. In addition to the above-mentioned force-displacement curve behaviour, the absorbed energy up to the shear strength W and the absorbed energy up to 80 % of the shear strength W_{80} were analyzed.

Prior of analyzing the effect of the process parameters, a correlation analysis is performed among the mechanical behaviour of FSSW joints. Figure 9a, b compare the absorbed energies and stiffness, with shear strength of FSSW joints produced with different processing conditions. Linear fit curves were reported (with their equations) to evaluate the correlations between absorbed energies and shear strength (Fig. 9a) as well as the correlation between stiffness and shear strength (Fig. 9b). The correlation between the above-mentioned quantities was evaluated by means of the coefficient of determination R^2, R^2 that ranges between 0 (no

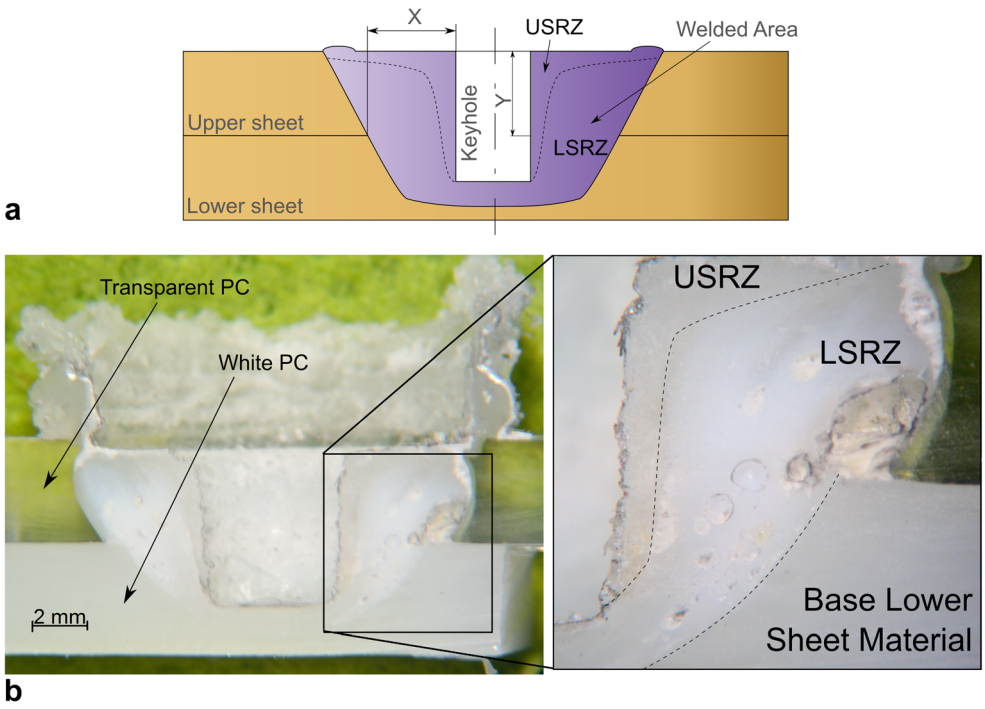

Fig. 6 **a** Schematic representation of the cross section of a friction stir spot weld. **b** cross section of a FSSW joint performed on transparent (*top-side*) and white (*bottom-side*) PC sheets highlighting the LSRZ-welded area

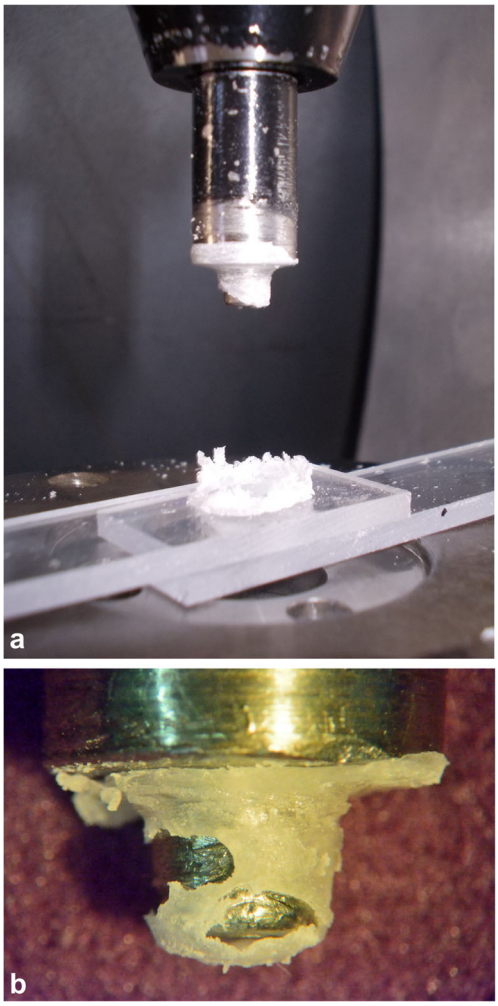

Fig. 7 Built-up-edge on the surface of the tool

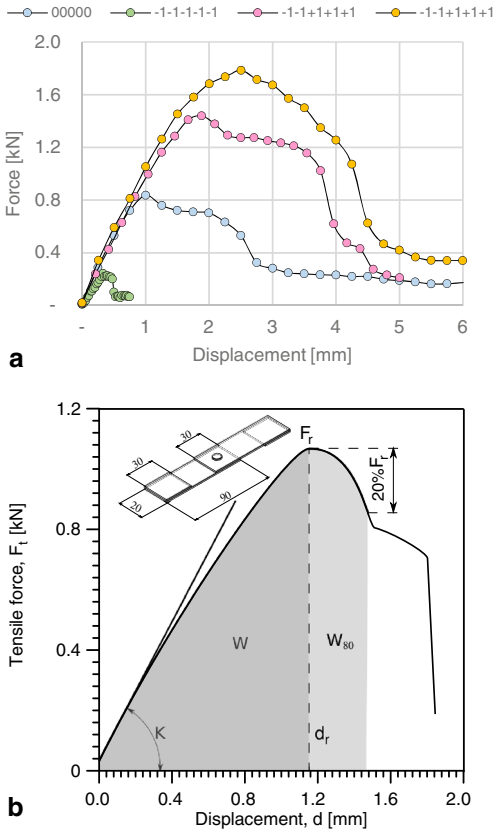

Fig. 8 **a** Force-displacement curve of joints produced under different processing conditions. **b** Main mechanical behaviour of welds measured during the tests and schematic representation of single lap shear test specimen

correlation) and 1 (perfect correlation). As can be seen, a high correlation exists between the absorbed energy W and the shear strength F_r since the high value of R^2=0.94, whilst weaker correlations exist between W_{80} and F_r as well as between K and F_r. As a result, the effect of the process parameters on W and F_r are very similar since they are highly correlated. By contrast, because of the low correlation between stiffness and shear strength, it should conduct separate analysis for the stiffness.

3.4 Influence of process parameters on mechanical behaviour of FSSW joints

3.4.1 2^5 Exploratory plan

The influence of the analyzed process parameters on the mechanical behaviour of produced FSSW joints is investigated by means of statistical analysis techniques, particularly main effects (Fig. 10a), interaction plots (Fig. 10b) as well as ANOVA analysis. Main effects plots show the average outcome for each level of each factor, combining the effects of the other factors as if all variables were independent. Interaction plots illustrate the effects between variables that are not independent.

The trend of the shear strength F_r is increasing with the processing times T_P, T_D and T_W, whilst it is decreasing with the processing speeds v_f and n, being highly sensitive to the factors "tool plunge rate" (v_f) and "Dwell time" (T_D). To better understand the effect of the process parameters on the mechanical behaviour of FSSW joints, the cross sections of relevant specimens are reported in Fig. 11, whereas Fig. 11a depicts the cross section of the reference configuration produced using middle levels for significant process parameters (v_f, n and T_D) and highest levels of T_P and T_W (Fig. 12).

When high plunging rates (v_f) are involved, a lower interaction time between the tool and material is produced resulting in lower material heating and mixing and consequently lower extension of welded region (as can be also noted by comparing Fig. 11a, c). Under higher rotational speeds (n), a high frictional heat is produced leading to a steep reduction in the material viscosity. The material is thus expelled from the welding region owing to centrifugal forces and indirect extrusion effect, as depicted in Fig. 13. As can

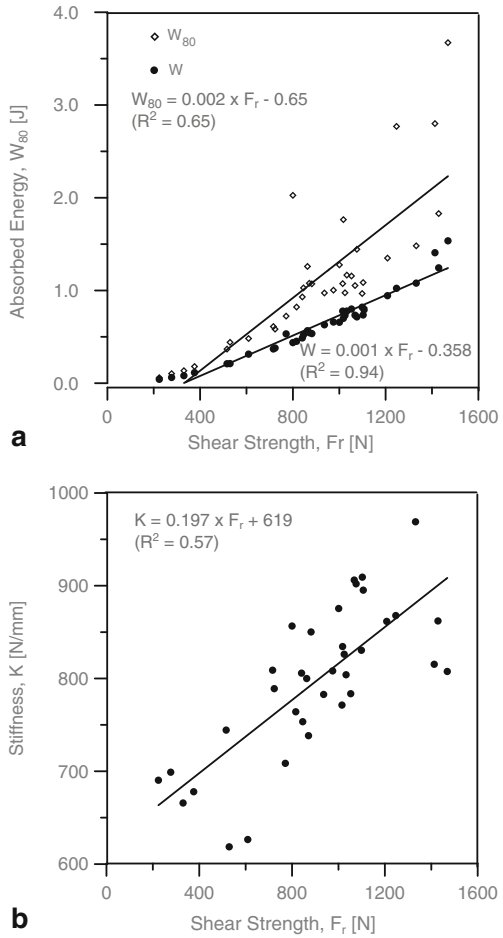

Fig. 9 **a** Correlation between absorbed energy and shear strength. **b** Correlation between stiffness and shear strength

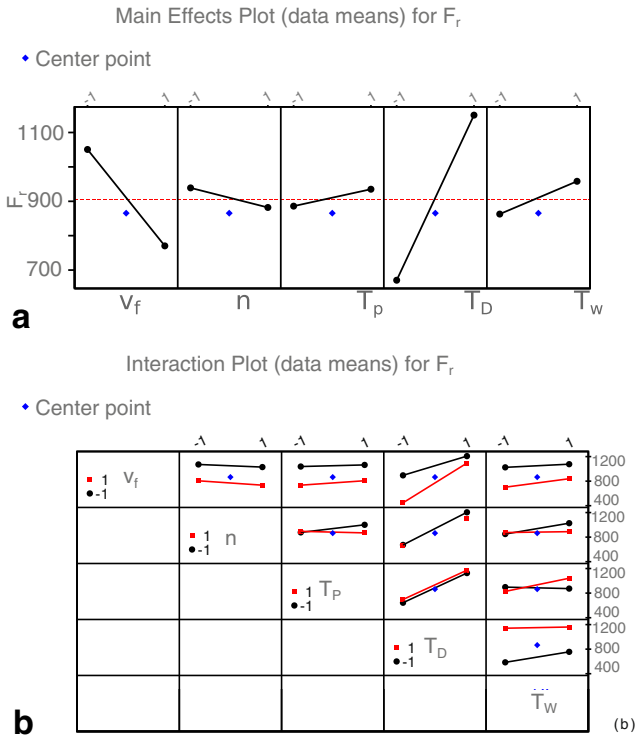

Fig. 10 **a** Main effects plot for tensile shear strength and **b** interaction effects plot for tensile shear strength

be observed, a material ring develops at the upper side of the joint owing to an ejection effect, which was particularly evident when high values of rotational speed were adopted. These results are in agreement with those reported in [25], (where the values n=500, 800 and 1250 rpm were adopted) which showed that the maximum strength was obtained for the intermediate level of rotational speed (n=800 rpm). Indeed, lower rotational speed (n=500 rpm) resulted in little friction; on the other hand, under the highest rotational speed (n=1250), excessive tool heating and high inertia forces were found. Such an ejecting effect reduced the material within the welding zone resulting in weaker joints. According to Fig. 10, the effect of pre-heating time T_P is negligible whilst the increase in dwell time T_D results in stronger joints. Indeed, prolonged dwell time results in longer tool-material interaction leading to a higher production of frictional heat. As a result, when high values of T_D parameter are involved, a larger area is molten (as can be observed in Figs. 11d and 12) leading to higher mechanical performances.

Although T_W has a lower influence, excessively low values of waiting time results in extreme reduction of shear strength. Indeed, a certain waiting time should be elapsed previous to proceed with the extraction of the punch in order to allow the decrease in the welded material temperature and avoid the tearing of the molten material from the rest of the sheets, as shown in Fig. 11e.

In order to evaluate quantitatively the significance of the factors and their interactions, the analysis of variance (ANOVA) of shear strength was carried out. The results of ANOVA analysis are reported in Table 2.

The significance of each source and coefficient was determined by Student's T test and P values, which are listed in Table 2. In this investigation, the desired level of confidence was considered to be 95 %. Values of P index lower than 0.05 indicate that the correspondent term is significant. In this case, all process parameters are significant. Dwell time was found to be the most effective factor influencing the weld strength, since its lowest P value. Then, tool plunge rate, waiting time and second-order interaction term between tool plunge rate and dwell time are found to be effective in weld strength, respectively.

The mechanical properties of friction stir welding spot connections are mainly influenced by the plunge rate, dwell time and rotational speed. Particularly, the highest shear strength (F_r=1470 N) was obtained by selecting low levels of tool plunge rate and tool rotational speed and high levels of preheating, dwell and waiting times. On the other hand, high levels of tool plunge rate and low levels of tool rotational

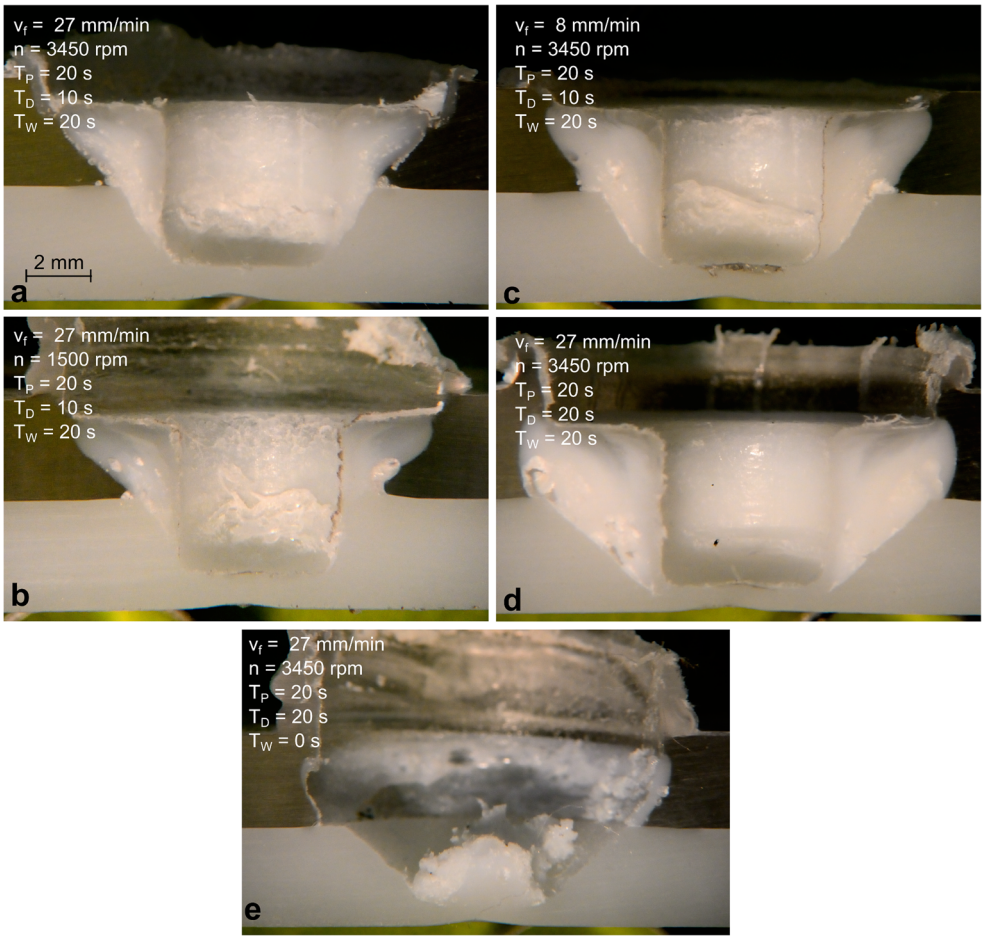

Fig. 11 Cross sections of FSSW joints produced under different processing conditions

speed, pre-heating, dwell and waiting times generated the joint with the worst mechanical behaviour (F_r=224 N). The cross sections of the joints exhibiting the highest and lowest mechanical strength are reported in Fig. 14. As can be observed, the joint with the highest strength has a large welded area (A_s= 31 mm^2) leading to a weld strength $\sigma_{weld}=F_r/A_s$=48 MPa. On the other hand, the welded area of the weaker joint is very small since the width X=0.1 mm.

To evaluate the effectiveness of the joining process as well as to compare the joint performances with that produced by other joining solutions, the weld factor f_w is utilized:

$$f_w = \frac{\sigma_{weld}}{\sigma_{base}} \quad (1)$$

where σ_{weld} and σ_{base} are the strengths of a weld and that of the base material. Therefore, the weld factor achieved under

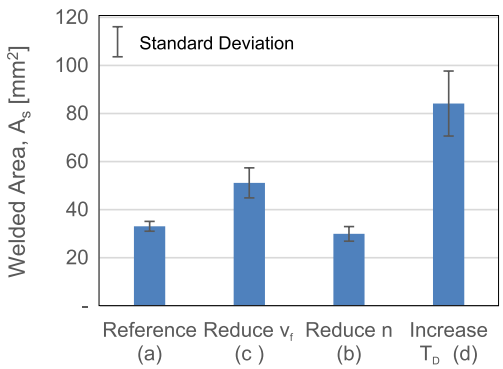

Fig. 12 Variation of welded area with relevant process parameters

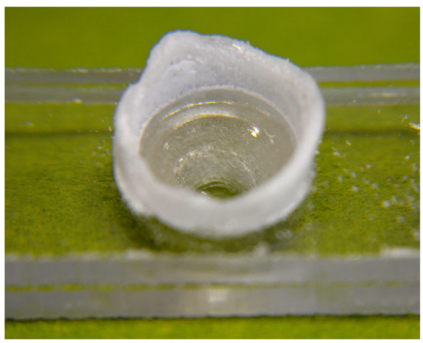

Fig. 13 Ejection effect owing to high values of n (specimen: −1+1+1+ 1+1)

Table 2 Analysis of variance for lap shear strength

Source	DF	SS	MS	F	P
Main effects	5	2,586,792	517,358	262.65	0.000
2-way interactions	10	521,249	52,125	26.46	0.003
3-way interactions	10	291,844	29,184	14.82	0.010
4-way interactions	5	61,597	12,319	6.25	0.050
5-way interactions	1	4255	4255	2.16	0.216
Residual error	4	7879	1970		
Curvature	1	7190	7190	31.31	0.011
Pure error		689	230		
Total	35	3,473,615			
Term	Effect	Coef	SE	T	P
Constant		905.5	7.397	122.41	0.000
v_f	−280.2	−140.1	7.846	−17.86	0.000
n	−56.8	−28.4	7.846	−3.62	0.022
T_P	49.3	24.7	7.846	3.14	0.035
T_D	479.7	239.8	7.846	30.57	0.000
T_w	95.3	47.7	7.846	6.07	0.004
$v_f \times n$	−14.4	−7.2	7.846	−0.92	0.410
$v_f \times T_P$	22.7	11.3	7.846	1.45	0.222
$v_f \times T_P$	166.8	83.4	7.846	10.63	0.000
$v_f \times T_w$	43.7	21.8	7.846	2.78	0.050
$n \times T_P$	−74.2	−37.1	7.846	−4.73	0.009
$n \times T_D$	−52.3	−26.2	7.846	−3.33	0.029
$n \times T_w$	−80.9	−40.5	7.846	−5.16	0.007
$T_p \times T_D$	−3.2	−1.6	7.846	−0.2	0.849
$T_p \times T_w$	119.2	59.6	7.846	7.6	0.002
$T_D \times T_w$	−75.4	−37.7	7.846	−4.81	0.009
$v_f \times n \times T_P$	5.2	2.6	7.846	0.33	0.758
$v_f \times n \times T_D$	2.8	1.4	7.846	0.18	0.866
$v_f \times n \times T_w$	−42.1	−21	7.846	−2.68	0.055
$v_f \times T_P \times T_D$	−6.1	−3	7.846	−0.39	0.719
$v_f \times T_P \times T_w$	−25.4	−12.7	7.846	−1.62	0.180
$v_f \times T_D \times T_w$	−76.3	−38.2	7.846	−4.86	0.008
$n \times T_P \times T_D$	79.6	39.8	7.846	5.07	0.007
$n \times T_P \times T_w$	−40.3	−20.2	7.846	−2.57	0.062
$n \times T_D \times T_w$	−35.4	−17.7	7.846	−2.26	0.087
$T_P \times T_D \times T_w$	137.7	68.8	7.846	8.77	0.001
$v_f \times n \times T_P \times T_D$	−53.8	−26.9	7.846	−3.43	0.027
$v_f \times n \times T_P \times T_w$	20.1	10	7.846	1.28	0.270
$v_f \times n \times T_D \times T_w$	−62.3	−31.2	7.846	−3.97	0.017
$v_f \times T_P \times T_D \times T_w$	−22.7	−11.3	7.846	−1.45	0.222
$n \times T_P \times T_D \times T_w$	1.9	1	7.846	0.12	0.908
$v_f \times n \times T_P \times T_D \times T_w$	23.1	11.5	7.846	1.47	0.216

optimal processing conditions is 0.8. Such a value is higher than that characterizing most of the competitive processes. In hot gas welding, typical values of weld factor, which highly depend on the polymer type, range between 0.45 and 0.82 for V-welds and 0.63 and 0.74 for X-welds [28]; nevertheless, employment of an external welding rod and precise substrate preparation (such as V and X-grooved profiles). As reported by Strand [29], the effectiveness of competitive joining processes are much lower than that achieved by FSW and FSSW processes; indeed, ultrasonic welding is characterized by f_w= 0.75 and a higher cost of the machine. Extrusion and hot-plate welding allow much higher weld factors f_w=0.70 and 0.90, respectively; however, such processes require the preparation of the weld edge (typically V-groove), and the cost of the machine are much higher than FSSW. On the other hand, adhesives allow a weld factor up to 0.90 and limited machine cost; however, they are characterized by fair repeatability, production of toxic fumes during use and cure phases, surface preparation including degreasing of the substrate and high sensitivity to worker skills. In the laser welding (LW) process, which allows to produce a weld strength comparable to that of the substrate [30], the employability of such a process is limited by the wavelength absorptivity coefficient of the polymer; in transmission laser welding, one of the components must be transparent and the other should absorb the laser radiation [31]; in order to apply the pressure in the weld zone, external clamping systems are involved [32].

3.4.2 Optimization 3^3 plan

According to the results achieved with the 2^5 exploratory plan, the shear strength (F_r) of friction stir spot-welded joints was mainly influenced by the tool plunge rate (v_f), and the dwell time (T_D). Tool rotation speed (n) seems to be less influent for the values adopted in the exploratory tests, but it affected the amount of the material ejected during the joining phase. In order to better understand the influence of the above-mentioned factors, a second series of experimental tests was conducted according to a 3^3 full factorial design of experiments, where tool rotational speed, tool plunge rate and dwell time were varied. The remaining factors, i.e. preheating and waiting time were kept constant to the high level (value=20 s), which are the ones which maximized the shear strength. Table 3 summarizes the welding parameters and the values employed in the 3^3 factorial plan.

In this case, the shear strength F_r can be expressed as:

$$F_r = f(v_f, n, T_D) \tag{2}$$

A second-order polynomial can be used to represent the influence of the process parameters on the shear strength of the joints, as follows:

$$F_r = b_0 + \sum b_i \cdot x_i + \sum b_{ii} \cdot x_i^2 + \sum b_{ij} \cdot x_i x_j \tag{3}$$

where b_0 is the average of the response and b_i, b_{ij} and b_{ii} are regression coefficients that depend on linear, interaction and

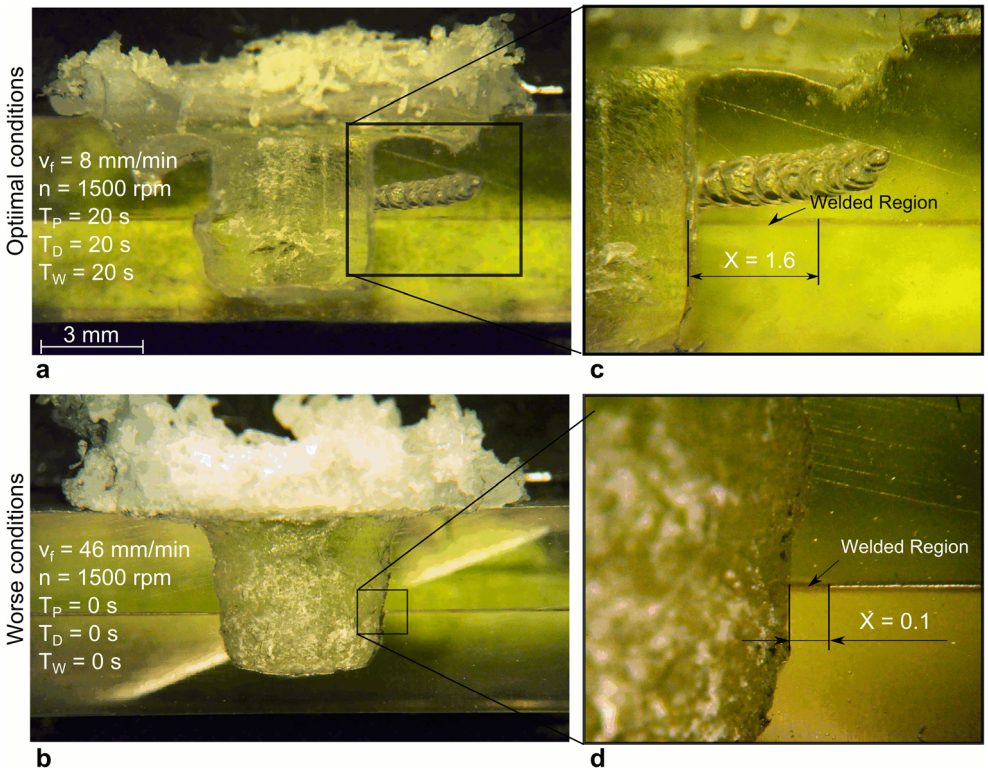

Fig. 14 Cross sections of joints produced under different processing conditions leading to: **a** highest strength and **b** lowest strength **c** enlargement of joint with the highest mechanical strength

squared terms of factor, respectively. Table 4 summarizes the analysis ANOVA of a second-order polynomial. As can be inferred, both the quadratic terms b_{ii} (except that for v_f) and the interaction terms b_{ij} have negligible influence on the joints shear strength since they have a P value higher than 0.05 whilst the linear terms b_i and the quadratic term of v_f are all significant. Therefore, the empirical equation involved only the terms having a P value lower than the adopted significance. As a result, Eq. 3 was derived:

$$F_r = 1525 - 28.2 \times v_f - 0.28 \times n + 11.4 \times \mathrm{TD} + 0.45 \times v_f 2 + 0.07 \times \mathrm{TD2} + 0.29 \times v_f \times \mathrm{TD}$$

The coefficient of determination R^2=0.76 confirms a relatively good agreement of the developed model with experimental data, as also confirmed by trends reported in Fig. 15a.

Table 3 Experimental factors and levels used in the 3^3 factorial plan

Welding parameter	Level 1	Level 2	Level 3
Tool plunge rate, v_f (mm/min)	8	27	46
Tool rotation speed, n (rpm)	1500	3450	5400
Dwell time, T_D (s)	0	10	20
T_P=T_W		20 s	

In Table 5, the analysis of variance for joints stiffness is presented.

Table 4 Analysis of variance for shear strength in the 3^3 full factorial design of experiments

Source	DF	SS	MS	F	P
Regression	9	1,559,796	173,311	5.98	0.001
Linear	3	1,230,168	410,056	14.14	0.000
Square	3	271,893	90,631	3.13	0.053
Interaction	3	57,735	19,245	0.66	0.586
Res. error	17	492,923	28,995		
Total	26	2,052,719			
Estimated regression coefficients					
Term	Coef	SE	T	P	
Constant	670.8	86.7	7.737	0.000	
v_f	−96.2	40.14	−2.397	0.028	
n	−102.9	40.14	−2.564	0.020	
T_D	220.2	40.14	5.487	0.000	
$v_f \times v_f$	160.9	69.52	2.314	0.033	
$n \times n$	139.2	69.52	2.003	0.061	
$T_D \times T_D$	6.9	69.52	0.099	0.922	
$v_f \times n$	−41.5	49.16	−0.844	0.410	
$v_f \times T_D$	55	49.16	1.119	0.279	
$n \times T_D$	8	49.16	0.163	0.873	

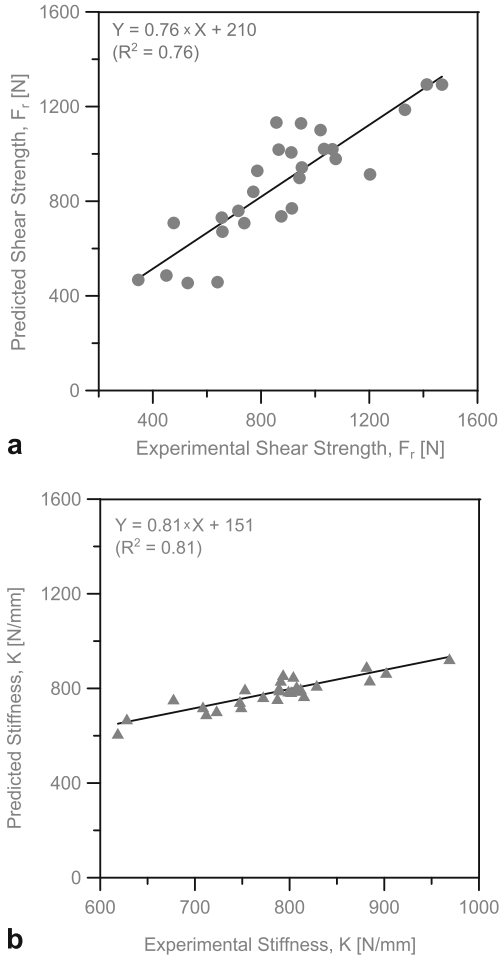

Fig. 15 Correlation graph between predicted and experimental values of **a** shear strength and **b** stiffness

By interpolating the experimental data of 3^3 factorial plane, the following equation for K was derived:

$$K = 949 - 0.9 \times v_f - 0.05 \times n - 13.4 \times \mathrm{TD} - 0.01 \times v_f 2 + 0.25 \times \mathrm{TD2} + 0.05 \times v_f \times \mathrm{TD} \quad (4)$$

Correlation between regression model and experimental values of joints stiffness are reported in Fig. 15b.

3.5 Prediction of shear strength by neural networks

Artificial neural networks have been employed in several fields of production engineering such as clinching [33], laser hardening [34], shape rolling [35], fused deposition [36], friction stir welding [37] etc. because of the capability to model complex nonlinear relationships between inputs and outputs. An artificial neural network (ANN) was developed to predict the shear strength of welded joints. A multi-layer perceptron (MLP) in which each neuron is fully connected with the neurons of neighbouring layers has been used in this work. In addition, each perceptron is characterized by nonlinear activation function such as hyperbolic tangent or sigmoid function. A back-propagation (BP) learning method has been adopted. BP consists of two steps, namely, propagation and weight update. During the forward propagation step, the network, on the basis of a guess of weights and biases, performs a forecast of the input samples (in the training set). Then, such predictions are compared with the corresponding output values to generate the deltas of all output and hidden layers (backward propagation). On the basis of the errors achieved, a gradient of the weight is computed; thus, a ratio of the gradient is therefore subtracted by the actual weight. Such a loop-procedure is reiterated to minimize the sum of squared errors (SSE).

Table 5 Analysis of variance for stiffness in the 3^3 full factorial design of experiments

Source	DF	SS	MS	F	P
Regression	9	125,192	13910.2	7.9	0.000
Linear	3	67,081	22360.4	12.7	0.000
Square	3	4283	1427.8	0.81	0.505
Interaction	3	53,827	17942.4	10.2	0.000
Estimated regression coefficients					
Term	Coef	SE	T	P	
Constant	764.6	21.365	35.787	0.000	
v_f	−37.7	9.89	−3.81	0.000	
n	−16	9.89	−1.615	0.130	
T_D	45.29	9.89	4.58	0.000	
$v_f \times v_f$	−4.88	17.13	−0.285	0.780	
$n \times n$	8.12	17.13	0.474	0.640	
$T_D \times T_D$	24.98	17.13	1.458	0.160	
$v_f \times n$	−8.92	12.113	−0.737	0.470	
$v_f \times T_D$	9.28	12.113	0.766	0.450	
$n \times T_D$	65.72	12.113	5.426	0.000	

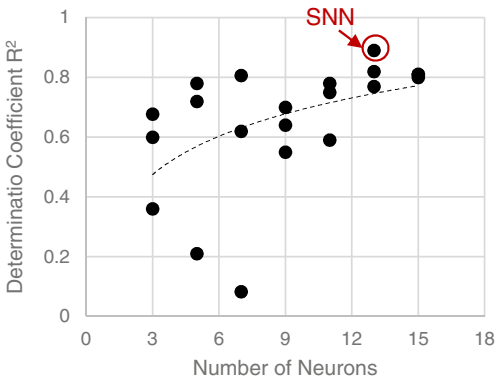

Fig. 16 Variation of determination coefficient achieved by ANNs with number of neurons in the hidden layer

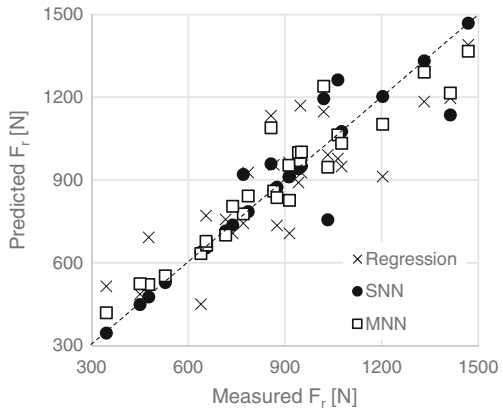

Fig. 17 Comparison among models predictions

In order to improve generalization and avoid overfitting, two approaches were tested, namely, early stopping and multiple neural networks (MNN). Early stopping method consists in dividing the available data in three subsets, namely, training (80 %), validation (10 %) and test (10 %). The training set is utilized to compute the gradient and update the weights and biases of the ANN. During the training process, the error on the validation subset decreases; however, as the network begins to overfit data in the training set, the error in the validation set begins to rise. Therefore, by monitoring the error of the validation set, it is possible to automatically stop the training of the ANN as overtraining occurs.

ANN generalization can be also improved (especially when the available dataset is small) by training multiple networks and averaging the outputs. In this case, each ANN is trained by using different subsets from the available data; the mean squared error of the averaged output will be likely lower than most of the singular networks (perhaps not all); however, the network will be able to generalize better when new data will be presented.

Two network configurations were employed: single neural network (SNN) which is that achieved the best performances in terms of correlation coefficient and average from multiple neural networks (MNN) which is attended to better generalize new data. In the case of MNN, the prediction was calculated as the average of the predictions from 10 ANNs.

The developed networks were characterized by three neurons in the input layer: tool plunge rate (v_f), the tool rotation rate (n) and the dwell time (T_D); a hidden layer; and one neuron in the output layer. To determine the number of

Table 6 Comparison of the mean square error (MSE), standard error (SE) and correlation coefficient (R^2)

	MSE	Standard error (SE)	R^2
Regression	20,427	127.0	0.73
SNN	9509	99.0	0.87
MNN	7882	79.9	0.9

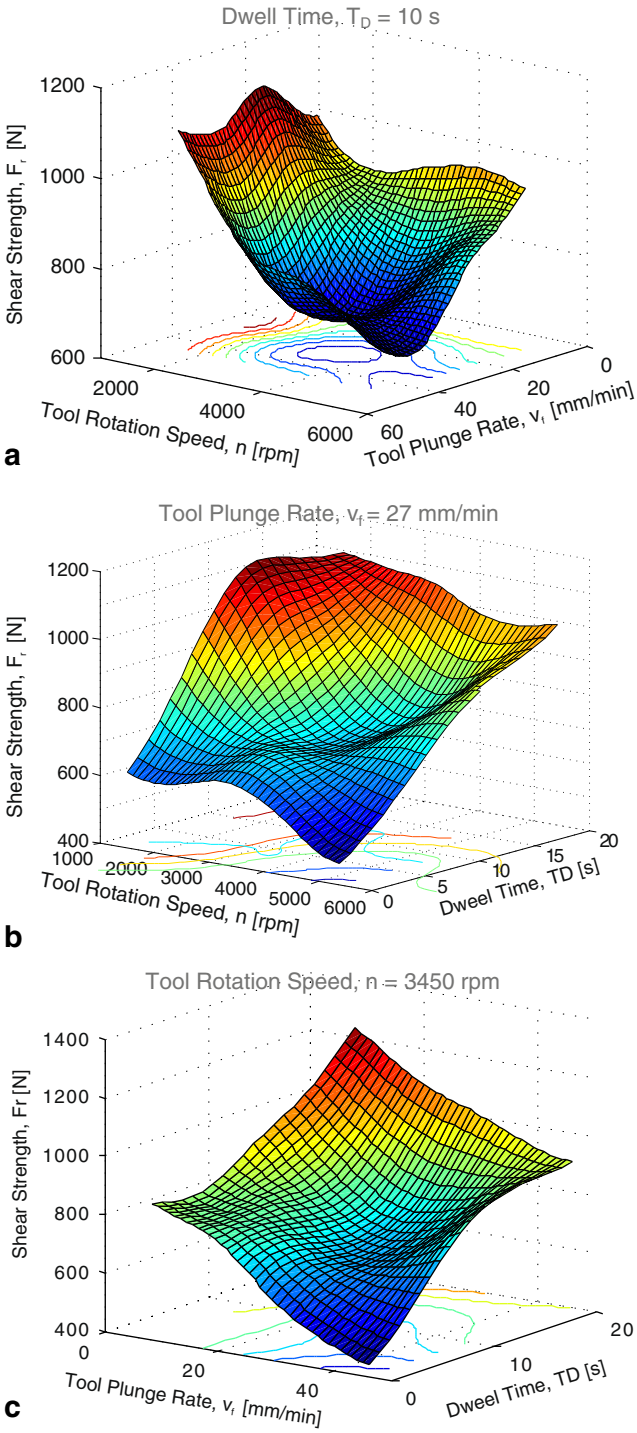

Fig. 18 Surface plots calculated by means of the MNN

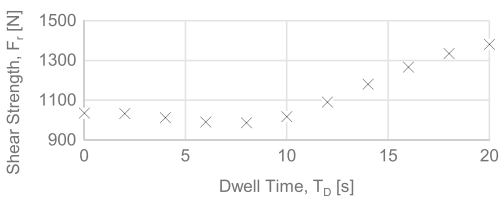

Fig. 19 Variation of shear strength (F_r) with dwell time with v_f=8 mm/min and n=1500 rpm

neurons in the hidden layer, preliminary tests were conducted by varying the hidden layer dimension. Figure 16 depicts the variation of the determination coefficient with the number of neurons in the hidden layer. As can be noted, the increase in the number of neurons results in an increase in the determination coefficient since the network can model more complex cases. However, using an excessive number of neurons causes a hurried convergence leading to a sudden stop of ANN training. For this reason, a hidden layer with 13 neurons was chosen as a compromise between these aspects.

Figure 17 depicts the fitting between the regression, SNN and MNN models and the experimental data. The MNN ensures a better fitting with a standard error (SE)=79.9 and a correlation coefficient R^2=0.90. The standard error is almost 20 % lower than that of SNN and 37 % lower than that of the regression model. A comparison of the mean square error (MSE), SE and correlation coefficient (R^2) is summarized in Table 6. As can be noted, the MNN is characterized by an improved generalization capability as compared to the SNN; in addition, it was found that the SNN poorly fitted the data outside the training dataset, the correlation coefficient of the validation and test datasets (R^2=0.95) being much lower than that of the training set (R^2=0.77).

Figure 18 depicts the surface plots calculated by means of the MNN. The surface plot are indicative of possible interactions among the analyzed process parameters and are built by considering one parameter in the middle level and the other two on the x and y axes. According to the plots, the maximum achievable shear strength, F_r, is 1.38 kN, corresponding to the process parameters: tool plunge rate v_f=8 mm/min, dwell time T_D=20 s and tool rotation rate n=1500 rpm.

A further analysis was carried out near the optimal conditions by varying the dwell time T_D over the investigated domain. Figure 19 depicts the variation of the joints' shear strength by adopting the optimal parameters for tool plunge rate (v_f=8 mm/min) and tool rotation speed (n=1500 rpm) and varying the dwell time T_D between 0 and 20 s. The shear strength is marginally influenced by T_D up to 10 s. Under this condition, the minimum value of the dwell time should be preferred in order to reduce the process time without affecting the joint strength. On the other hand, for T_D>10 s, the joint strength increases almost linearly with dwell time, allowing an increase of the shear strength by 38 % for T_D=20 s.

4 Conclusions

Friction stir spot welding of polycarbonate sheets was analyzed by means of experimental, statistical and artificial intelligence techniques. The effect of tool rotational speed, tool plunge rate, pre-heating time, dwell time and waiting time on mechanical properties and weld geometry of FSSW joints were investigated. The adoption of optimized process conditions allowed achieving shear strength in the welded area close to that of the base material. The following results were achieved by the experimental tests:

- Mechanical behaviour and geometry of the welded region of FSSW joints are highly influenced by processing speeds and processing times.
- The effect of pre-heating time on the mechanical behaviour of FSSW joints is negligible.
- The tool plunge rate, the dwell time and the waiting time highly influence the joint strength of polycarbonate FSSW; in particular, the dwell time was the most dominant welding parameter.
- A certain waiting time must be elapsed before proceeding with the extraction of the punch from the sheets to avoid the removal of the welded (still pasty) material.
- The tool rotational speed has a minimum influence on the joint strength, resulting in a small decrease of tensile shear strength with increasing the speed in the range of values adopted in the experimental tests.
- The developed neural network model allowed to predict the shear strength according to the process conditions.
- The process conditions which maximized the weld's shear strength were determined.
- The results show that an increase in the weld's strength by almost ten times can be achieved by optimizing the processing times and processing speeds.

References

1. Azarsa E, Mostafapour A (2013) On the feasibility of producing polymer–metal composites via novel variant of friction stir processing. J Manuf Process 15(4):682–688
2. Bilici MK (2012) Application of Taguchi approach to optimize friction stir spot welding parameters of polypropylene. Mater Des 35:113–119
3. Lambiase F, Di Ilio A (2015) Mechanical clinching of metal–polymer joints. J Mater Process Technol 215:12–19
4. Lee C-J, Lee J-M, Ryu H-Y, Lee K-H, Kim B-M, Ko D-C (2014) Design of hole-clinching process for joining of dissimilar materials—Al6061-T4 alloy with DP780 steel, hot-pressed 22MnB5 steel, and carbon fiber reinforced plastic. J Mater Process Technol 214:2169–2178
5. Gerstmann T, Awiszus B (2014) Recent developments in flat-clinching. Comput Mater Sci 81:39–44
6. Liu FC, Liao J, Nakata K (2014) Joining of metal to plastic using friction lap welding. Mater Des 54:236–244
7. Goushegir SM, dos Santos JF, Amancio-Filho ST (2014) Friction spot joining of aluminum AA2024/carbon-fiber reinforced poly(phenylene sulfide) composite single lap joints: microstructure and mechanical performance. Mater Des 54:196–206
8. D'Aniello M, Portioli F, Landolfo R (2014) Lap shear tests on hot-driven steel riveted connections strengthened by means of C-FRPs. Compos Part B 59:140–152

9. Amancio-Filho ST, dos Santos JF (2009) Joining of polymers and polymer-metal hybrid structures: recent developments and trends. Polym Eng Sci 49(8):1461–1476
10. Blaga L, Bancilă R, dos Santos JF, Amancio-Filho ST (2013) Friction Riveting of glass–fibre-reinforced polyetherimide composite and titanium grade 2 hybrid joints. Mater Des 50:825–829
11. Abibe AB, Amancio-Filho ST, dos Santos JF, Hage E (2013) Mechanical and failure behaviour of hybrid polymer–metal staked joints. Mater Des 46:338–347
12. Amancio-Filho ST, Bueno C, dos Santos JF, Huber N, Hage E (2011) On the feasibility of friction spot joining in magnesium/fiber-reinforced polymer composite hybrid structures. Mater Sci Eng A 528(10–11):3841–3848
13. Rai R, De A, Bhadeshia HK, DebRoy T (2011) Review: friction stir welding tools. Sci Technol Weld Join 16:325–343
14. Nandan R, Debroy T, Bhadeshia H (2008) Recent advances in friction-stir welding—process, weldment structure and properties. Prog Mater Sci 53(6):980–1023
15. Gerlich A, Su P, North TH (2005) Tool penetration during friction stir spot welding of Al and Mg alloys. J Mater Sci 40(24):6473–6481
16. Hancock R (2004) Friction welding of aluminium cuts energy cost by 99 %. Weld J 83(2):40–46
17. Sun YF, Shen JM, Morisada Y, Fujii H (2014) Spot friction stir welding of low carbon steel plates preheated by high frequency induction. Mater Des 54:450–457
18. Wang DA, Lee SC (2007) Microstructures and failure mechanisms of friction stir spot welds of aluminum 6061-T6 sheets. J Mater Process Technol 186(1–3):291–297
19. Gibson BT, Lammlein DH, Prater TJ, Longhurst WR, Cox CD, Ballun MC, Dharmaraj KJ, Cook GE, Strauss AM (2014) Friction stir welding: process, automation, and control. J Manuf Process 16(1):56–73
20. Wan L, Huang Y, Lv Z, Lv S, Feng J (2014) Effect of self-support friction stir welding on microstructure and microhardness of 6082-T6 aluminum alloy joint. Mater Des 55:197–203
21. Bagheri A, Azdast T, Doniavi A (2013) An experimental study on mechanical properties of friction stir welded ABS sheets. Mater Des 43:402–409
22. Bilici MK, Yukler AI (2012) Effects of welding parameters on friction stir spot welding of high density polyethylene sheets. Mater Des 33:545–550
23. Paoletti A, Lambiase F (2015) Optimization of friction stir welding of thermoplastics. Procedia CIRP 14 (in press)
24. Bilici MK, Yükler Aİ, Kurtulmuş M (2011) The optimization of welding parameters for friction stir spot welding of high density polyethylene sheets. Mater Des 32(7):4074–4079
25. Simões F, Rodrigues DM (2014) Material flow and thermo-mechanical conditions during friction stir welding of polymers: literature review, experimental results and empirical analysis. Mater Des 59:344–351
26. Dashatan SH, Azdast T, Ahmadi SR, Bagheri A (2013) Friction stir spot welding of dissimilar polymethyl methacrylate and acrylonitrile butadiene styrene sheets. Mater Des 45:135–141
27. Armagan A, Senol M (2008) Friction stir spot welding of polypropylene. J Reinf Plast Compos 27:2001–2004
28. Oliveira PHF, Amancio-Filho ST, dos Santos JF, Hage E (2010) Preliminary study on the feasibility of friction spot welding in PMMA. Mater Lett 64(19):2098–2101
29. Balkan O, Demirer H, Yildirim H (2008) Morphological and mechanical properties of hot gas welded PE, PP and PVC sheets. J Achievements Mater Manuf Eng 31(1):60–70
30. Strand S (2003) Joining plastics - can friction stir welding compete? Paper presented at the electrical insulation conference and electrical manufacturing &; coil winding technology conference, 2003. Proceedings 23-25 Sept. 2003
31. Shin HM, Choi HW (2014) Design of energy optimization for laser polymer joining process. Int J Adv Manuf Technol 75(9–12):1569–1576
32. Aden M, Mamuschkin V, Olowinsky A, Glaser S (2014) Influence of titanium dioxide pigments on the optical properties of polycarbonate and polypropylene for diode laser wavelengths. J Appl Polym Sci 131(7):1–5
33. Ilie M, Cicala E, Grevey D, Mattei S, Stoica V (2009) Diode laser welding of ABS: experiments and process modeling. Opt Laser Technol 41(5):608–614
34. Lambiase F, Di Ilio A (2013) Optimization of the clinching tools by means of integrated FE modeling and artificial intelligence techniques. Procedia CIRP 12:163–168
35. Lambiase F, Di Ilio AM, Paoletti A (2013) Prediction of laser hardening by means of neural network. Procedia CIRP 12:181–186
36. Lambiase F (2013) Optimization of shape rolling sequences by integrated artificial intelligent techniques. Int J Adv Manuf Technol 68(1–4):443–452
37. Peng A, Xiao X, Yue R (2014) Process parameter optimization for fused deposition modeling using response surface methodology combined with fuzzy inference system. Int J Adv Manuf Technol